

Optical properties of Er³⁺-Ag co-doped ZnO nanocrystals prepared by combustions method

Jinmei Yang · Haiming Zhang · Xu Wang ·
Feifei Qin · Caixia Wang

Received: 7 May 2014 / Accepted: 16 June 2014 / Published online: 16 July 2014
© Springer Science+Business Media New York 2014

Abstract The Er³⁺-Ag co-doped ZnO nanocrystals have been synthesized by citric acid-assisted combustions method. The effect of different concentration of silver nanoparticles (NPs) on Er³⁺ doped ZnO nanocrystals and the optical behaviors are explored. The nanocrystals were characterized by X-ray diffractions, scanning electron microscopy, UV-Vis-NIR absorption spectra, X-ray photoelectron spectroscopy, and photoluminescence, respectively. The luminous intensity of Er³⁺ doped ZnO nanocrystals was significantly influenced by the concentration of silver NPs. A large enhancement in up-conversion intensity has been observed when the concentration of silver NPs was 0.10 mol%. The effect of localized surface plasmon resonance of silver NPs and the energy transfer between the silver NPs and Er³⁺ ions (²H_{11/2} → ⁴I_{15/2}, ⁴S_{3/2} → ⁴I_{15/2}, and ⁴F_{9/2} → ⁴I_{15/2}) are discussed as the sources of enhancement or quenching.

1 Introduction

Recently, the synthesis and characterizations of semiconductors co-embedded with rare earth (RE) and metallic nanoparticles (NPs) have attracted numerous interests because of their great application in sensing, solar cells, light emitting diodes, surface enhanced Raman spectroscopy (SERS), and single-molecular spectroscopy [1–4]. It is generally known that ZnO has been used as a host material for the visible and infrared emissions of various RE ions, because it is possessed of the wide band gap of

3.37 eV at room temperature and large exciton binding energy [5, 6]. As for these, it has wide application in electronic and optical materials. For example, ZnO combined with Cu₂O films has also been used to realize solar cell [7]. The unfilled 4f shells of REs make them a promising candidate to achieve the up-conversions (UC) emissions due to the excited state absorptions, energy transfer UC process and cross relaxations emissions by favorable nonradiative decay mechanisms [8]. The Er³⁺ ions is the most widely studied among the RE ions that show up-conversions photoluminescence (UC-PL) because it provides the long lived intermediate level ⁴I_{11/2} easily accessible with a diode laser at 980 nm. Er³⁺ doped ZnO nanocrystals have been proved as reliable materials for infrared detections, laser diodes, optical amplifiers as well as fluorescent labels for sensitive detections of biomolecules [9–11].

The Er³⁺ doped ZnO has been reported by many literatures [12, 13]. For example Lee et al. reported ZnO:Er thin films by rf magnetron sputtering to improve the Infrared emission, although the UC emissions of Er³⁺ doped ZnO was realized, the efficiency of UC emissions is still low. Therefore, immense efforts have been dedicated to enhance the efficiency of UC emissions. As it is known to all, the metallic NPs and Er³⁺ co-doped ZnO show an effective improvement of UC emissions efficiency. Confinement of excitations wavelength by metallic NPs contributes to a strong field enhancement through the excitations of the collective oscillations of electron clouds called localized surface plasmon (LSP) effect. The surface plasmon has been found to enhance the luminescent efficiency with the merit of easily tuning the resonance band by suitable structural properties such as shape, size, number density of the metal NPs, distance between the RE ions and the metallic surface and dielectric host environment,

J. Yang (✉) · H. Zhang · X. Wang · F. Qin · C. Wang
School of Science, Tianjin Polytechnic University,
Tianjin 300387, China
e-mail: y0709470@126.com

allowing the field enhancement in wide energy ranges [14, 15].

In this study, the Er^{3+} -Ag co-doped ZnO nanocrystals have been synthesized by citric acid (CA)-assisted combustions method. The effect of different concentration of silver NPs on Er^{3+} doped ZnO nanocrystals and the optical behaviors have been detailed studied and explained.

2 Experimental details

ZnO powders doped with Er^{3+} concentration being 2.0 mol% and different molar content of AgNO_3 (0, 0.05, 0.10, 0.15, 0.2, 0.3 mol%) were prepared by a combustions method. $\text{Zn}(\text{NO}_3)_2 \cdot 6\text{H}_2\text{O}$, $\text{Er}(\text{NO}_3)_3 \cdot 5\text{H}_2\text{O}$ and AgNO_3 are used in the powder form as starting materials in different mol%’s. The following compositions are used:

- 98.00 $\text{Zn}(\text{NO}_3)_2 \cdot 6\text{H}_2\text{O}$ -2.0 $\text{Er}(\text{NO}_3)_3 \cdot 5\text{H}_2\text{O}$ -0.0 AgNO_3 .
- 97.95 $\text{Zn}(\text{NO}_3)_2 \cdot 6\text{H}_2\text{O}$ -2.0 $\text{Er}(\text{NO}_3)_3 \cdot 5\text{H}_2\text{O}$ -0.05 AgNO_3 .
- 97.90 $\text{Zn}(\text{NO}_3)_2 \cdot 6\text{H}_2\text{O}$ -2.0 $\text{Er}(\text{NO}_3)_3 \cdot 5\text{H}_2\text{O}$ -0.10 AgNO_3 .
- 97.85 $\text{Zn}(\text{NO}_3)_2 \cdot 6\text{H}_2\text{O}$ -2.0 $\text{Er}(\text{NO}_3)_3 \cdot 5\text{H}_2\text{O}$ -0.15 AgNO_3 .
- 97.80 $\text{Zn}(\text{NO}_3)_2 \cdot 6\text{H}_2\text{O}$ -2.0 $\text{Er}(\text{NO}_3)_3 \cdot 5\text{H}_2\text{O}$ -0.20 AgNO_3 .
- 97.70 $\text{Zn}(\text{NO}_3)_2 \cdot 6\text{H}_2\text{O}$ -2.0 $\text{Er}(\text{NO}_3)_3 \cdot 5\text{H}_2\text{O}$ -0.30 AgNO_3 .
- 99.90 $\text{Zn}(\text{NO}_3)_2 \cdot 6\text{H}_2\text{O}$ -0.0 $\text{Er}(\text{NO}_3)_3 \cdot 5\text{H}_2\text{O}$ -0.10 AgNO_3 .

The ingredient chemicals [$\text{Zn}(\text{NO}_3)_2 \cdot 6\text{H}_2\text{O}$, $\text{Er}(\text{NO}_3)_3 \cdot 5\text{H}_2\text{O}$ and AgNO_3] were dissolved into 20 mL of deionized water at 60 °C with constant stirring. Then citric acid was added to the solutions with the mole ratio of ($\text{Zn}^{2+} + \text{Er}^{3+} + \text{Ag}^+$) to citric acid to be 1:3, and then $\text{NH}_3 \cdot \text{H}_2\text{O}$ was slowly added to adjust pH value to 7.0. The resulting solution was heated in air at 100 °C for 2 h to evaporate the solvent and obtained the xerogels. Then, it was transformed into a crucible and calcined in air at 800 °C for 30 min. And lastly, the mixture was cooled down to room temperature in the furnace. The doped ZnO sintered was milled into powder for structural analysis and spectral measurement.

The crystalline structure of the samples was determined by using XRD (D8 Advance powder diffractometer with Cu $\text{K}\alpha$ radiations). The size and morphology of the samples were examined by filed emission scanning electron microscopy (SEM, 1530VP). X-ray photoelectron spectroscopy (XPS) measurements were done on a VG Multilab-2000 \times system with Al $\text{K}\alpha$ source and a charge neutralizer. All the binding energies were referenced to the C 1s peak at 284.8 eV of the surface adventitious carbon. Lambda-35 scanning spectrophotometer is employed to measure UV-Vis-NIR absorption spectra in the range 300–1,100 nm. The Photoluminescence (PL) spectra of the samples were measured with Spectrophotometer (FL3-2-IR320-NIR-TCSPC) by using 325 nm line of Xe lamp as excitations source at room temperature. The light source is a diode laser emitting NIR wavelength at 980 nm with full width at half

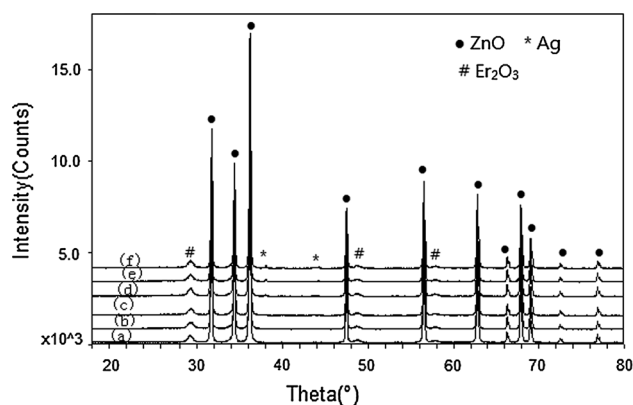


Fig. 1 The XRD patterns of Er^{3+} -Ag co-doped ZnO nanocrystals with different concentration of silver NPs: 0 mol% (a), 0.05 mol% (b), 0.10 mol% (c), 0.15 mol% (d), 0.2 mol% (e), 0.3 mol% (f)

maximum of 2 nm. Room temperature UC-PL spectrum was collected by a SPEX1000 M spectrometer with a spectral resolution of 0.3 nm and was detected by a photomultiplier tube which was attached to the spectrometer.

3 Results and discussions

Figure 1 illustrates the XRD patterns of Er^{3+} -Ag co-doped ZnO nanocrystals with different concentration of silver NPs. The main diffraction peaks are well indexed to ZnO with hexagonal wurtzite structure. The result indicates that the structure of ZnO is not altered by the presence of Er^{3+} and Ag in these samples. All of the diffraction peaks from ZnO are in good agreement with the standard values for the highly crystalline ZnO crystals (JCPDS No. 36-1451) [16]. The weak impurity peaks at 29.2°, 48.7°, and 57.9° can be assigned to Er_2O_3 [17]. Er_2O_3 phase being detected implies that some Er_2O_3 precipitated from ZnO host. Furthermore, as can be seen in Fig. 1, an obvious diffraction peak at 38.0° assigned to the Ag(0) appears, when the concentration of silver NPs rises to 0.15 mol%.

Figure 2a shows SEM images of Er^{3+} -Ag co-doped ZnO nanocrystals, which display rod and particles-like morphology. Figure 2b shows the spherical Ag NPs are observed in the ZnO surface gathered granulated when the concentrations of silver NPs was 0.20 mol%, which are about 298 nm in diameter.

Figure 3a shows the XPS full spectrum of Er^{3+} -Ag co-doped ZnO nanocrystals. The XPS peaks not only contain Zn, O, Er and Ag elements but also C, carbon element mainly comes from pump oil in the vacuum system of the XPS instrument itself. It indicates that Er^{3+} -Ag co-doped ZnO nanocrystals are only composed of four elements, Zn, O, Er and Ag, which are consistent with the above XRD results. The high-resolutions spectra for Zn, O, Er and Ag

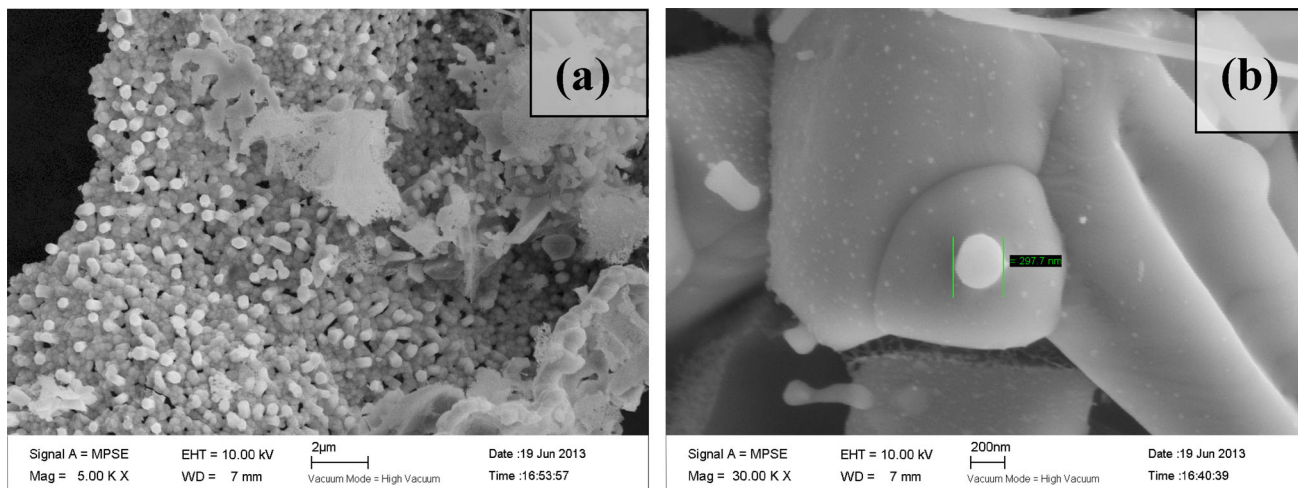


Fig. 2 SEM images of Er^{3+} -Ag co-doped ZnO nanocrystals (a) and spherical Ag NPs (b)

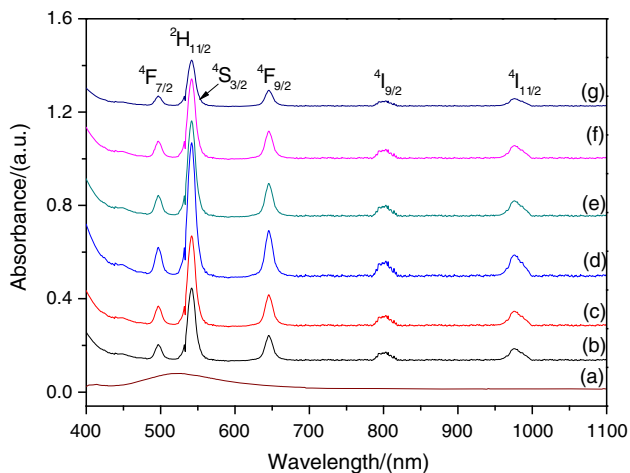


Fig. 3 UV-vis-IR absorption spectra of Er^{3+} -Ag co-doped ZnO nanocrystals: 0.10 mol% Ag–0 mol% Er (a), 0 mol% Ag–2.0 mol% Er (b), 0.05 mol% Ag–2.0 mol% Er (c), 0.10 mol% Ag–2.0 mol% Er (d), 0.15 mol% Ag–2.0 mol% Er (e), 0.20 mol% Ag–2.0 mol% Er (f), 0.30 mol% Ag–2.0 mol% Er (g)

are shown in Fig. 3b–e respectively. The peaks observed at 1,045.8 and 1,022.7 eV, which can be seen in Fig. 3b and are assigned to Zn $2p_{1/2}$ and Zn $2p_{3/2}$, can be attributed to the Zn^{2+} oxidations state according to reported XPS data [18]. In Fig. 3c, two asymmetrical peaks can be observed in the O_{1s} profile and can be divided into two symmetrical peaks (531.4 and 532.6 eV), indicating that two different kinds of O element in the Er^{3+} -Ag co-doped ZnO nanocrystals. The peak at 531.4 eV should be attributed to O_{1s} of ZnO nanocrystals [19], and another peak is from the hydroxyl absorbed on the surface of the products. The Er 4d signal presents a complex shape, related to the coupling phenomena between the 4d hole and the lanthanide partially filled 4f shell. In particular, negligible variations in the positions and the shape of the most intense $4d_{5/2}$ spin-

orbit split component at 169.6 eV indicate the same electronic structures of Er(III) species, which can be seen in Fig. 3d [20, 21]. The peaks appearing in Fig. 3e can be attributed to Ag $3d_{5/2}$ (368.1 eV) and Ag $3d_{3/2}$ (374.2 eV), respectively, which indicates the formations of metal Ag (0) [22]. It is in agreement with the XRD results.

Figure 4 shows the absorption spectra of samples without silver NPs and with different concentration of silver NPs such as 0.05, 0.10, 0.15, 0.20, and 0.30 mol% silver NPs. The peaks at 980, 800, 655, 522 and 488 nm are assigned to $^4I_{11/2}$, $^4I_{9/2}$, $^4F_{9/2}$, $^2H_{11/2}$ and $^4F_{7/2}$, energy levels of Er^{3+} ions respectively. It is evident that the most intense transition is $^2H_{11/2}$. The UV-Vis-NIR absorption spectrum is the most reliable tool to analyze the formation of metallic NPs and surface plasmon resonance (SPR) absorption bands. The absorption spectrum of Ag doped ZnO nanocrystals (Fig. 4a) shows prominent plasmon absorption band (530 nm) characteristic of Ag NPs.

Figure 5 shows the room-temperature PL spectra of Er^{3+} doped ZnO nanocrystals with different concentration of silver NPs under a 325 nm Xe laser excitations. It is found that all individual curves show two similar emissions bands, including a narrow UV band around 394 nm, corresponding to the near band edge (NBE) emissions of ZnO, and a broad visible band locating in the range of 440–630 nm, which can be assigned to surface states or oxygen vacancies [23, 24]. The luminous intensity of Er^{3+} -Ag co-doped ZnO nanocrystals was obviously influenced by the concentrations of silver NPs. The luminous intensities of Er^{3+} -Ag co-doped ZnO nanocrystals with different concentrations of silver NPs vary in the following order: 0.10 mol% > 0.05 mol% > 0 mol% > 0.15 mol% > 0.20 mol% > 0.30 mol%. As is shown in Fig. 3, the visible emission is stronger than UV emissions. In this work, the visible emission intensity increased by about two times as compared with Er^{3+} doped ZnO nanocrystals

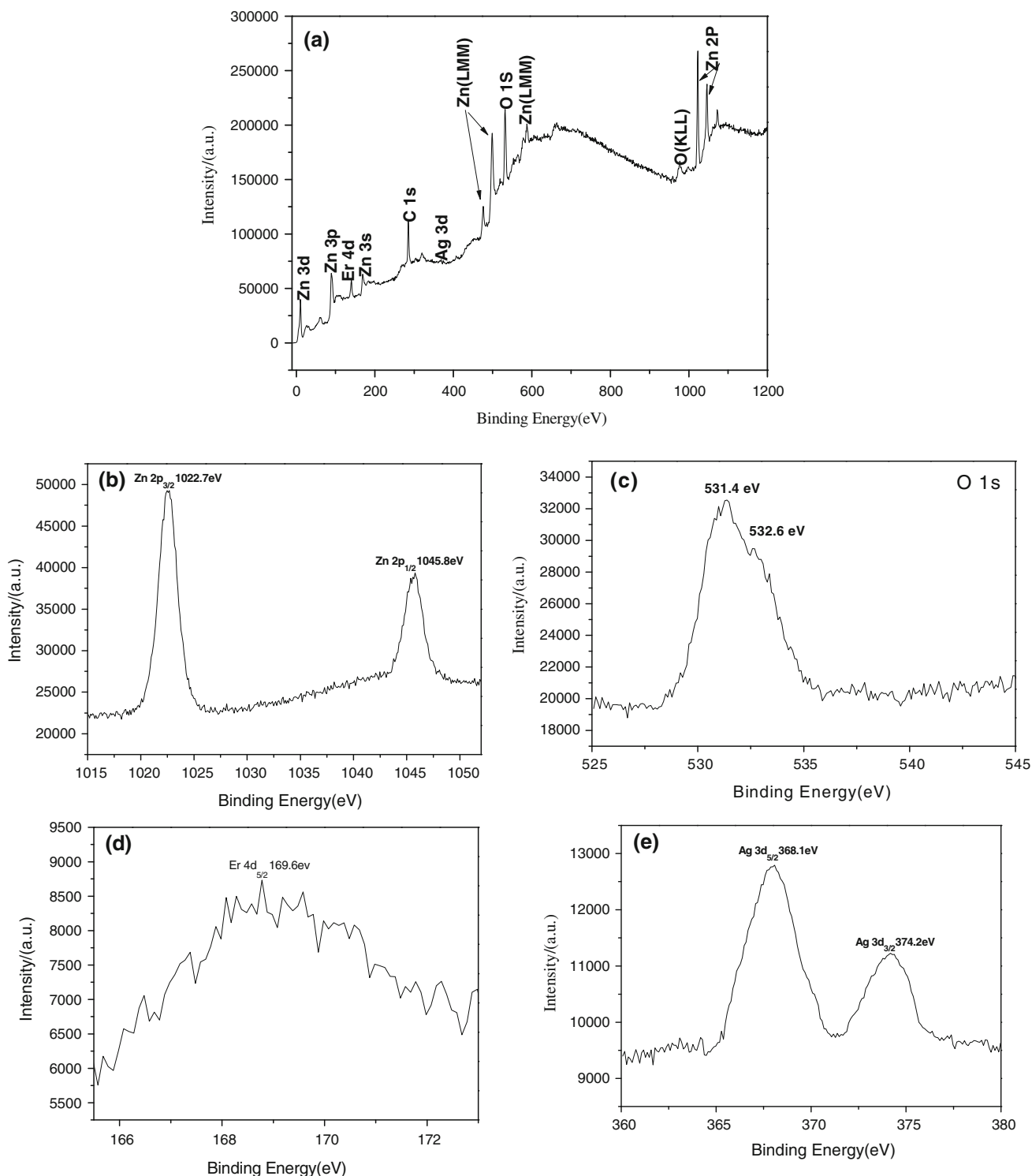


Fig. 4 **a** The XPS full spectrum of the Er^{3+} -Ag co-doped ZnO nanocrystals (0.20 mol%). The high-resolutions spectra for Zn, O, Er, and Ag species are shown in **(b)**, **(c)**, **(d)**, and **(e)**, respectively

when the concentrations of silver NPs was 0.10 mol%. It is caused by the LSP resonance effect of silver NPs [25]. Along with the increasing concentrations of silver NPs, the luminous intensity significantly weakened.

Figure 6 shows UC luminescence spectra of Er^{3+} -Ag co-doped ZnO nanocrystals with different concentration of silver NPs under direct excitations at 980 nm at room temperature. The green emissions ranging from 520 to

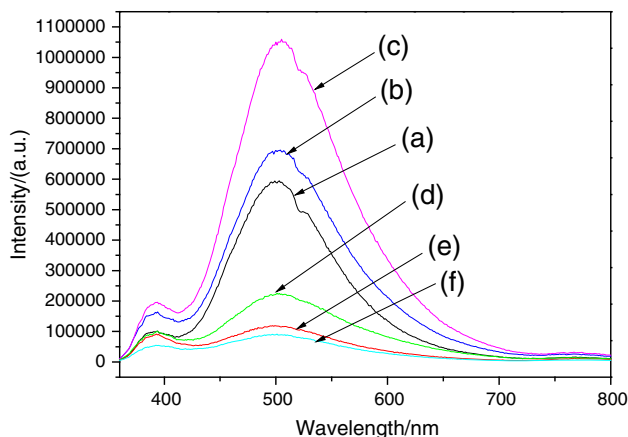


Fig. 5 PL spectra of Er³⁺-Ag co-doped ZnO nanocrystals with different concentration of silver NPs under direct excitations at 325 nm at room temperature: 0 mol% (a), 0.05 mol% (b), 0.10 mol% (c), 0.15 mol% (d), 0.20 mol% (e), 0.30 mol% (f)

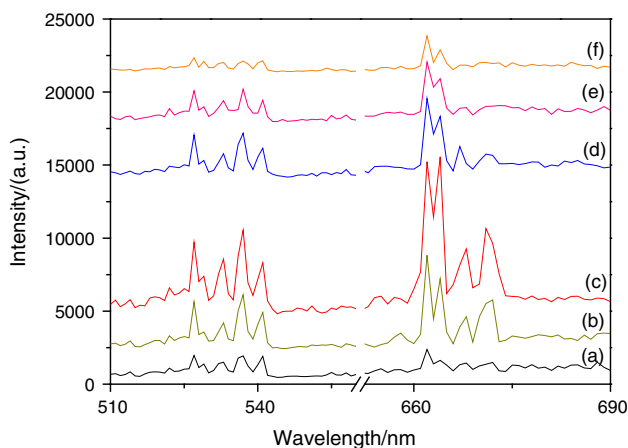


Fig. 6 UC luminescence spectra of Er³⁺-Ag co-doped ZnO nanocrystals with different concentration of silver NPs under direct excitations at 980 nm at room temperature: 0 mol% (a), 0.05 mol% (b), 0.10 mol% (c), 0.15 mol% (d), 0.20 mol% (e), 0.30 mol% (f)

565 nm is due to the ²H_{11/2}, ⁴S_{3/2} → ⁴I_{15/2} transitions, and the red emissions from 640 to 690 nm is associated with the ⁴F_{9/2} → ⁴I_{15/2} transitions of Er³⁺ ions [11]. It is clear that UC luminescence intensity enhanced drastically after embedding the silver NPs into the Er³⁺ doped ZnO nanocrystals. The integrated red and green emissions intensities are shown in Fig. 7. In Fig. 7, the green emissions intensity is lower than that of the red emissions. Once increasing the concentrations of silver NPs, the red emissions intensity increased steadily until the concentration of silver NPs reached 0.10 mol%, which was 3.8 times enhanced, beyond which the intensity decreased. However, the green emissions spectral intensity has a little change when compared to the red one. And the relation between integral intensity of green and red UC emissions and the different

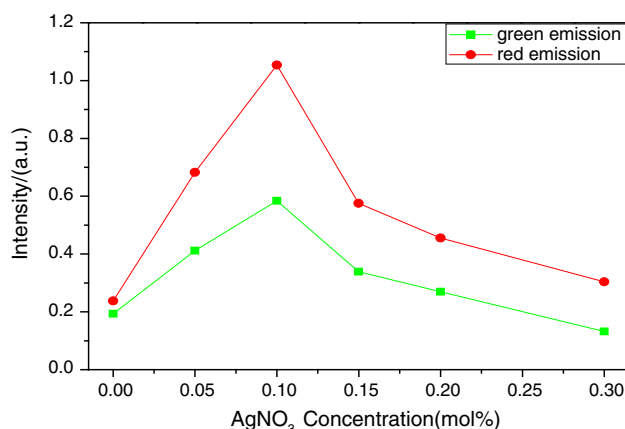


Fig. 7 Integral intensity of green and red emission as a function of the different concentration of silver NPs (Color figure online)

concentration of silver NPs has the same trend with the separate green and red UC emissions.

The schematic energy levels diagram of Er³⁺-Ag co-doped ZnO nanocrystals under 980 nm excitations is shown in Fig. 8. The UC luminescence mechanism comprises several processes, including excited-state absorptions (ESA) and energy transfer (ET) between silver NPs and Er³⁺ ions. The green emissions produced by transitions of ²H_{11/2}, ⁴S_{3/2} → ⁴I_{15/2} of Er³⁺. The ²H_{11/2} and ⁴S_{3/2} levels are mainly populated by the excited state absorptions (ESA), energy transfers (ET), and subsequently non-radiative decay to the ²H_{11/2} and ⁴S_{3/2} states. About the red emissions by transitions of ⁴F_{9/2} → ⁴I_{15/2} of Er³⁺, the population of level is ascribed mainly to ET and the cross relaxations (CR) process. The LSPR enhances the local electric field in vicinity of Er³⁺ ions which results to increment in absorptions of Er³⁺ ions and radiative decay rate of upper levels [26], which lead to enhance the UC emissions. The distance between the emitter ions (Er³⁺) and the NP, the particle size, and the relative value of the dielectric functions of the silver NPs and the host determined whether enhancement or quenching occurs [27–29]. With increasing the concentrations of silver NPs, the quantity and size of NP is more and bigger. Therefore, local electric field and emissions intensities are increased and enhanced effectively. Enhanced local field is the major factor to yield the efficient UC luminescence in “hot spots” [30], while an energy transfer from silver NPs to Er³⁺ ions is also probable as the second channel to enhance the UC of Er³⁺ ions. By increasing the concentrations of silver NPs, and growth in more quantity of silver NPs, an energy transfer from Er³⁺ ions to metallic surface will be also probable. Consequently, a quenching in UC emissions takes place. Given these facts, there are several ways to improve the film quality in the future. Firstly, we can change the Er concentration. Secondly, the combustions

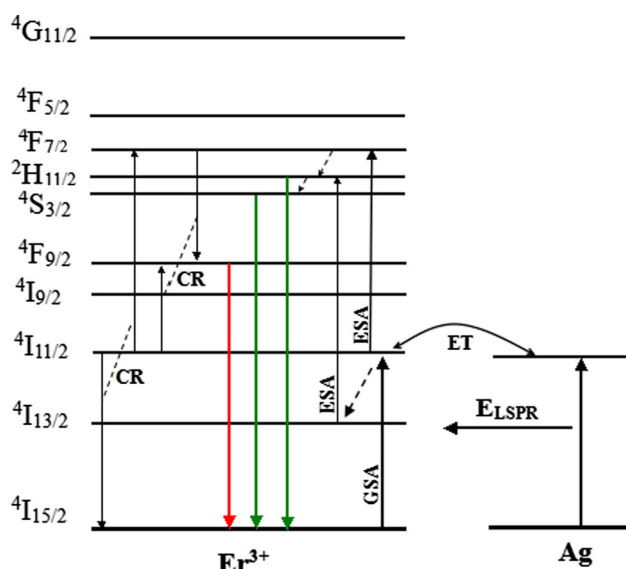


Fig. 8 Schematic energy levels diagram of Er³⁺ ions in the Ag doped ZnO nanocrystals and UC luminescence processes under 980 nm excitations

temperature can be adjusted to obtain the best quality. Lastly, we can choose different chelating agents to pick up the proper one.

4 Conclusions

In conclusion, the Er³⁺–Ag co-doped ZnO nanocrystals were prepared by citric acid (CA)-assisted combustions method. The luminous intensity of Er³⁺ doped ZnO nanocrystals was significantly influenced by the concentrations of silver NPs. The effect of different concentration of silver nanoparticles (NPs) on Er³⁺ doped ZnO nanocrystals and the optical behaviors are examined. A large enhancement in UC luminous of Er³⁺–Ag co-doped ZnO nanocrystals was measured (3.8 times), which contributed to the LSP resonance of silver NPs as well as the energy transfer from silver NPs to Er³⁺ ions. The quenching of visible emissions is caused by an energy transfer from Er³⁺ ions to surface of large silver NPs for the concentrations of silver NPs more than 0.10 mol%. Introduction of silver NPs to Er³⁺ doped ZnO nanocrystals raise to the large enhances in the up-conversions luminous in the visible regions. The studied nanocrystals have practically excellent optical potential application in optical and medical devices.

Acknowledgments The authors gratefully acknowledge the financial support from the National Natural Science Foundations of China (No. 61274064).

References

1. J.W. Lo, W.C. Lien, C.A. Lin, J.H. He, Appl. Mater. Interfaces **3**, 1009 (2011)
2. L. Dolgov, V. Reedo, V. Kiisk, S. Pikker, I. Sildos, J. Kikas, Opt. Mater. **32**, 1540 (2010)
3. B.S. Cao, Y.Y. He, Z.Q. Feng, M. Song, B. Dong, Chinese J. Inorg. Chem. **27**, 776 (2011)
4. X.Q. Liu, F. Li, Y.Q. Wang, H.Y. Jin, H. Wang, Z. Li, Mater. Lett. **94**, 19 (2013)
5. A.K. Pradhan, K. Zhang, G.B. Loutts, U.N. Roy, Y. Cui, A. Burger, J. Phys. Condens. Mater. **16**, 7123 (2004)
6. G. Blasse, B.C. Grabmaier, *Luminescent Materials* (Springer, Berlin, 1994)
7. Z.G. Zang, A. Nakamura, J. Temmyo, Opt. Express **21**, 11448 (2013)
8. A. Patra, C.S. Friend, R. Kapoor, P.N. Prasad, Appl. Phys. Lett. **83**, 284 (2003)
9. G.S. He, P.P. Markowicz, T.C. Lin, P.N. Prasad, Nature **415**, 767 (2002)
10. J.S. Lee, Y.J. Kim, Ceram. Int. **38S**, 585 (2012)
11. X. Wang, X.G. Kong, G.Y. Shan, Y. Yu, Y.J. Sun, L.Y. Feng, K.F. Chao, S.Z. Lu, Y.J. Li, J. Phys. Chem. B **108**, 18408 (2004)
12. J.S. Lee, Y.J. Kim, Ceram. Int. **38**, S585 (2012)
13. X. Wang, X.G. Kong, Y. Yu, Y.J. Sun, H. Zhang, J. Phys. Chem. C **111**, 15119 (2007)
14. R.J. Amjad, M.R. Sahar, S.K. Ghoshal, M.R. Dousti, S. Riaz, B.A. Tahir, J. Lumin. **132**, 2718 (2012)
15. V.A.G. Rivera, S.P.A. Osorio, D. Manzani, Y. Messaddeq, L.A.O. Nunes, E. Marega Jr, Opt. Mater. **33**, 888 (2011)
16. American Society for Testing and Material. *Powder Diffractions Files; Joint Committee on Powder Diffractions Standards* (Swarthmore, PA, 1999), pp. 3–888
17. Y.J. Sun, Y. Chen, L.J. Tian, Y. Yu, X.G. Kong, Q.H. Zeng, Y.L. Zhang, H. Zhang, J. Lumin. **128**, 15 (2008)
18. W.Q. Peng, S.C. Qu, G.W. Cong, Z.G. Wang, Cryst. Growth Des. **6**, 1518 (2006)
19. C.W. Yen, M.A. Mahmoud, M.A. El-Sayed, J. Phys. Chem. A **113**, 4340 (2009)
20. L. Armelao, D. Barreca, G. Bottaro, A. Gasparotto, D. Leonarduzzi, C. Maragno, E. Tondello, C. Sada, J. Vac. Sci. Technol. A **24**, 1941 (2006)
21. W.C. Lang, B.D. Padalia, L.M. Watson, D.J. Fabian, P.R. Norris, Faraday Discuss Chem. Soc. **60**, 37 (1975)
22. S.J. Chang, M. Li, Q. Hua, L.J. Zhang, Y.S. Ma, B.J. Ye, W.X. Huang, J. Catal. **293**, 195 (2012)
23. J. Wang, P. Liu, X. Fu, Z. Li, W. Han, X. Wang, Langmuir **25**, 1218 (2009)
24. K. Vanheusden, C.H. Seager, W.L.N. Warren, D.R.N. Tallant, J. Voigt, Appl. Phys. Lett. **68**, 403 (1996)
25. V.M. Shalaev, S. Kawata, *Nanophotonics with Surface Plasmons* (Elsevier, Amsterdam, 2007)
26. J. Zhu, K. Zhu, L. Chen, J. Non-Cryst. Solids. **352**, 150 (2006)
27. L.R.P. Kassab, C.B. de Araújo, R.A. Kobayashi, R. de Almeida, D.M. da Silva, J. Appl. Phys. **102**, 103515 (2007)
28. J.N. Farahani, D.W. Pohl, H.J. Eisler, B. Hecht, Phys. Rev. Lett. **95**, 017402 (2005)
29. A. Chiasera, M. Ferrari, M. Mattarelli, M. Montagna, S. Pelli, H. Portales, J. Zheng, G.C. Righini, Opt. Mater. **27**, 1743 (2005)
30. T. Som, B. Karmakar, Solid State Sci. **13**, 887 (2011)